

1 **Genetic architecture drives seasonal onset of hibernation in the 13-lined**
2 **ground squirrel**

3 Katharine R. Grabek, Thomas F. Cooke, L. Elaine Epperson, Kaitlyn K. Spees, Gleyce F.
4 Cabral, Shirley C. Sutton, Dana K. Merriman, Sandra L. Martin and Carlos D. Bustamante

5
6 **Short title: Genetic architecture of hibernation onset**

7
8 **Author Affiliations**

9 Katharine R. Grabek

10 *Email: krgrabek@stanford.edu

11 Affiliations: Department of Genetics and Department Biomedical Data Science, Stanford
12 University School of Medicine, Stanford, California, United States of America

13
14 Thomas F. Cooke

15 Affiliation: Department of Genetics, Stanford University School of Medicine, Stanford,
16 California, United States of America

17
18 L. Elaine Epperson

19 Affiliation: Center for Genes, Environment and Health, National Jewish Health, Denver,
20 Colorado, United States of America

21
22 Kaitlyn K. Spees

23 Affiliation: Department of Genetics, Stanford University School of Medicine, Stanford,
24 California, United States of America

25
26 Gleyce F. Cabral

27 Affiliations: Brazil Scientific Mobility Program, Science Without Borders Fellow/CAPES,
28 CAPES Foundation, Ministry of Education of Brazil, Brasília, DF, Brazil; Department of
29 Genetics, Stanford University School of Medicine, Stanford, California, United States of
30 America

31
32 Shirley C. Sutton

33 Affiliation: Department of Genetics and Department of Cardiovascular Medicine, Stanford
34 University School of Medicine, Stanford, California, United States of America

35
36 Dana K. Merriman

37 Affiliation: Department of Biology, University of Wisconsin Oshkosh, Oshkosh, Wisconsin,
38 United States of America

39
40 Sandra L. Martin

41 Affiliation: Department of Cellular and Developmental Biology, University of Colorado School of
42 Medicine, Aurora, Colorado, United States of America

43
44 Carlos D. Bustamante

45 *Email: cdbustam@stanford.edu
46 Affiliations: Department of Genetics and Department of Biomedical Data Science, Stanford
47 University School of Medicine, Stanford, California, United States of America; Chan
48 Zuckerberg Biohub, San Francisco, California, United States of America

49 **Abstract**

50 Hibernation is a highly dynamic phenotype whose timing, for many mammals, is
51 controlled by a circannual clock and accompanied by rhythms in body mass and food intake.
52 When housed in an animal facility, 13-lined ground squirrels exhibit individual variation in the
53 seasonal onset of hibernation, which is not explained by environmental or biological factors,
54 such as body mass and sex. We hypothesized that underlying genetic architecture instead
55 drives variation in this timing. After first increasing the contiguity of the genome assembly, we
56 therefore employed a genotype-by-sequencing approach to characterize genetic variation in
57 153 13-lined ground squirrels. Combining this with datalogger records, we estimated high
58 heritability (61-100%) for the seasonal onset of hibernation. After applying a genome-wide
59 scan with 46,996 variants, we also identified 21 loci significantly associated with hibernation
60 emergence, which alone accounted for 54% of the variance in the phenotype. The most
61 significant marker (SNP 15, $p=3.81 \times 10^{-6}$) was located near *prolactin-releasing hormone*
62 *receptor (PRLHR)*, a gene that regulates food intake and energy homeostasis. Other
63 significant loci were located near genes functionally related to hibernation physiology, including
64 *muscarinic acetylcholine receptor M2 (CHRM2)*, involved in the control of heart rate, *exocyst*
65 *complex component 4 (EXOC4)* and *prohormone convertase 2 (PCSK2)*, both of which are
66 involved in insulin signaling and processing. Finally, we applied an expression quantitative loci
67 (eQTL) analysis using existing transcriptome datasets, and we identified significant ($q < 0.1$)
68 associations for 9/21 variants. Our results highlight the power of applying a genetic mapping
69 strategy to hibernation and present new insight into the genetics driving its seasonal onset.

70

71 **Introduction**

72 Hibernation is a highly dynamic phenotype that maximizes energy savings during
73 periods of low resource availability. For a number of mammals, such as the 13-lined ground
74 squirrel, *Ictidomys tridecemlineatus*, an endogenous circannual clock controls the timing of
75 winter hibernation, along with rhythms in reproductive behavior, body mass, and food intake [1-
76 3]. These hibernators partition their year between two distinct states, homeothermy and
77 heterothermy (a.k.a hibernation, Fig 1A) that are distinguished by dramatic differences in
78 behavior and physiology. While physiology during homeothermy resembles that of a non-
79 hibernating mammal, squirrels spend most of their hibernation time in an energy-conserving
80 state called torpor (Fig 1B, top right). Here, metabolic, respiratory and heart rates are

81 dramatically reduced to 1-9% of homeothermic baselines, while body temperature is lowered
82 to near freezing [4]. However, torpor is not continuous, but instead punctuated by brief,
83 metabolically intense, arousals that largely restore baseline physiology, including near-
84 homeothermic body temperature [5,6]. Thus, hibernation is a period of heterothermy
85 composed of cycles between torpor and arousal.

86 The seasonal transition from homeothermy to heterothermy occurs during the autumn of
87 each year. Successful hibernation requires preparation, most notably the storage of large
88 amounts of energy in the form of fat, because this species fasts throughout the heterothermic
89 period. While post-reproduction homeothermy is marked by increased food intake, as the
90 onset of heterothermy approaches, the squirrel's metabolic rate slows, peak body mass is
91 achieved, and food intake ceases [7]. At the cellular level, glucose-based metabolism is
92 switched to one that is primarily lipid-based, and lipogenesis is swapped for lipolysis [8]. While
93 peak plasma insulin concentration occurs during this period, paradoxically, animals also
94 become transiently insulin-resistant [9]. At the mRNA and protein levels, sweeping changes in
95 expression are observed [10-14]. However, the genetic factors driving this transition remain
96 largely unknown.

97 The commencement of torpor, defined by a criterion drop in body temperature, is one
98 readily quantifiable outcome of the transition that marks the start of seasonal heterothermy.
99 When housed under standard laboratory conditions in an animal facility (Fig 1B, bottom), 13-
100 lined ground squirrels exhibit individual variation in the timing of their first bout of torpor. This
101 variation is neither accounted for by environmental signals, such as food withdrawal, shortened
102 photoperiod, or falling ambient temperature, nor by biological factors, such as age, body mass,
103 and sex. All of these variables have little to modest influence on timing [15]. Rather, consistent
104 with being controlled by an endogenous circannual clock, we hypothesized that observed
105 variation in the onset of torpor is due to underlying genetic variation between individuals. If so,
106 applying a genome-wide scan could potentially identify genetic components driving the start of
107 seasonal heterothermy.

108 Therefore, in this study, we first increased the contiguity of the 13-lined ground squirrel
109 draft genome assembly. We next employed a genotype-by-sequencing strategy to characterize
110 genetic variation in 153 13-lined ground squirrels whose tissues were previously collected for
111 use in transcriptomic, proteomic and biochemical studies [16-22]. Many of these squirrels were
112 surgically implanted with body temperature dataloggers, and from their records, we recorded

113 the first day that torpor occurred in each individual (Fig 1C). We next estimated the heritability
114 of, and identified genetic variants associated with, the onset of autumn torpor in this species.
115 Finally, we integrated data from prior transcriptomic studies to identify transcripts whose
116 expression levels were significantly associated with these variants. Our results present new
117 insight into the genetics driving the transition from homeothermy to heterothermy and illustrate
118 the power of genetic analysis to attack questions of exceptional biological significance in a
119 non-classical genetic model organism.

120

121 **Results**

122 *Long-range scaffolding of the draft genome assembly*

123 At the time this study began, the existing 13-lined ground squirrel genome assembly
124 (like that of many non-model organisms) contained thousands of unordered scaffolds, which
125 could lead to difficulties in identifying causative variants, as peaks in linkage disequilibrium
126 (LD) could be spread across multiple scaffolds. We therefore first sought to increase the
127 genome's contiguity using a long-range scaffolding technique [23].

128 A single library was constructed using proximity ligation of in vitro reconstituted
129 chromatin. After sequencing, which provided 52.6x physical coverage of the genome (Table 1)
130 and scaffolding, the contiguity of the final HiRise assembly was increased approximately three-
131 fold as compared to the existing draft assembly (N50 of 22.6Mb vs 8.19Mb; Table 1, Fig S1
132 and Table S1). The longest scaffold increased from 58.28Mb to 73.92Mb. Importantly, 539
133 original draft assembly scaffolds were reduced to just 33 scaffolds, which now contained half of
134 the genome (Fig S2).

135

136 **Table 1. Details of the draft assembly compared to the HiRise assembly.**

Assembly details	Draft	HiRise
Average coverage	495.1x	52.6x
Total length (Mb)	2,478.4	2,478.4
Contigs		
No. of contigs	153,485	153,521
Contig N50 (kb)	44.137	44.131
Scaffolds		
No. of scaffolds (≥ 0)	12,483	10,007
Longest scaffold (Mb)	58.28	73.93
Scaffold N50 (Mb)	8.19	22.6
No. of scaffolds \geq N50	80	33
Scaffold N90 (Mb)	1.13	3.33
Gaps		

Number of gaps	141,005	143,517
Percent of genome in gaps	6.75%	6.76%

137

138 *Identification of genetic variants*

139 We next applied a modified ddRAD sequencing protocol previously described in [24] to
140 generate libraries for 153 13-lined ground squirrels from which we obtained DNA from frozen
141 tissue. After aligning the resulting sample library reads to the HiRise genome assembly (Table
142 S2), we retained 337,695 loci (50.65 Mbp) that fell between predicted *BglIII* and *DdeI* target
143 regions, with coverage of at least one read in one individual. Applying variant calling and
144 filtering to these loci (Fig S3), we next identified 786,453 biallelic variants, which had an overall
145 Ti/Tv ratio of 2.19, comparable to ratios reported within intronic and intergenic regions [25]. For
146 use in downstream analyses, we retained 575,178 variants for which genotypes were present
147 in at least 90% of the individuals. Of these retained variants, 35,257 were indels, whereas
148 539,921 were single nucleotide polymorphisms.

149

150 *Population Structure and Genetic Relatedness*

151 The squirrels genotyped in this study originated from wild stock trapped in disparate
152 geographical locales (Fig 1D). The records for their exact source and relatedness were not
153 always available. This was not due to intentional sampling design, but rather due to the
154 availability of squirrels each year, either trapped from the wild or supplied from a breeding
155 colony, and the biological questions originally being pursued. Therefore, to identify population
156 structure within our sample set, we applied ADMIXTURE clustering with 5-fold cross validation
157 [26] on $K=2$ through $K=10$ ancestral populations using a set of 54 unrelated individuals who
158 best represented the ancestries of all squirrels (Fig S4; see Methods). We then applied
159 ADMIXTURE projection to estimate proportions of learned ancestries within the remaining 99
160 squirrels. The lowest cross validation error occurred at $K=3$ (Fig 2A, top plot), where individuals
161 separated into Colorado (CO), Illinois (IL) and Wisconsin (WI) components. The pairwise
162 genetic distance (F_{ST}) estimates between populations were 0.47 and 0.31 for CO vs. WI and
163 IL, respectively, and 0.30 for WI vs. IL, indicating moderate to strong genetic drift. The
164 individual home range for a 13-lined ground squirrel is 0.01 – 0.05 km² [27]. Observed genetic
165 differences may simply be due to isolation by geographic distance [28].

166 At $K=6$, we observed separation most consistent with records about sampling (Fig 2A,
167 bottom plot). For instance, the algorithm identified a La Crosse, WI (LaX) ancestral component
168 for the squirrels supplied from the UW Oshkosh breeding colony in 2010, matching the
169 breeding records for that year. Additionally, the algorithm identified two ancestral components
170 for the IL squirrels: those purchased in 2006 ('06) belonged to a single ancestry, while those
171 from 2010 ('10) segregated into another ancestry, suggesting different trapping locales
172 between years. While records about the origins of the UW Oshkosh squirrels supplied prior to
173 2010 were unavailable, the algorithm identified two ancestral components for this breeding
174 colony. The pairwise F_{ST} values were still consistently high (0.33-0.48) among all populations
175 (Table S3), except for the two (non-LaX) within Oshkosh (0.16) and the two within IL (0.23),
176 again supporting the notion of limited gene flow at increased geographical distance.

177 The first three principal components (PCs) from a PCA-based analysis recapitulated
178 both the observed ADMIXTURE $K=6$ clustering and the known geographical sampling locales
179 of the squirrels (Fig 2B). All populations were distinctly separated, except for the two within
180 Oshkosh, whose separation was only observed at the higher PCs (PC17 and PC19, Fig S5).

181

182 *Genetic relatedness within the Oshkosh breeding colony*

183 Due to the strong population structure, and hence large differences in allele
184 frequencies, we limited further analysis to just the Oshkosh population of squirrels (not
185 including LaX, $n=119$), for which we were able to collect the most phenotypic measurements
186 ($n=72$, Table S4) from analysis of the body temperature telemetry data, as opposed to fewer
187 than $n=10$ phenotypic measurements in each of the remaining populations. Our existing
188 records from the breeding colony suggested that many of these squirrels were littermates,
189 although exact relatedness was unknown. We therefore estimated relatedness, adjusting for
190 population substructure with the first PC [29,30], which distinguished the two ancestral
191 components (Fig 2C). Using pedigree reconstruction [31], we identified 19 first-degree families,
192 to which 80% of the squirrels belonged. Consistent with our records, most of these families
193 were composed solely of littermates (Fig 2D, right plot), although in some cases we also
194 identified parent-offspring relationships (Fig 2D, left plot).

195

196 *Heritability Estimates for Timing of Autumn Torpor Immersion*

197 We next investigated the effect of genetic architecture on autumn torpor onset within the
 198 Oshkosh subset of animals. We estimated heritability of this trait using a linear mixed model, in
 199 which we controlled for sex, year of monitoring and date of placement into the hibernaculum
 200 (our fixed effects, see methods), and we input the genetic relatedness estimates as the
 201 random effect. Unexpectedly, this model converged with no residual error in the variance
 202 components, resulting in an estimate of 100% heritability (LMM, Table 2). To confirm this high
 203 estimate, we fit a separate Bayesian multivariate general linearized mixed model with the
 204 same fixed and random effects. Here, the posterior mode of heritability was 99%, and the
 205 confidence intervals were between 61% and 99.9% (MCMCgrm, Table 2); even the lower
 206 bound of the estimate still indicated high heritability, confirming our hypothesis that underlying
 207 genetic architecture drives variation in the onset of torpor.

208

209 **Table 2. Estimates of heritability for the timing of the first of torpor bout in autumn.**

Trait	Sample Size (<i>n</i>)	Method	Fixed Effects	Fixed Effects R ²	Genetic variance	Error variance	Genetic Proportion	C.I. (95%)
Timing of torpor onset	72	LM		0.2505	--	--	--	--
		LMM	Sex, year, T _a	--	57.06	0.00	1	1-1
		MCMCgrm		--	49.8	0.41	0.99	0.61-0.99

210 T_a, ambient temperature ≤ 14°C, denotes day of placement of into hibernaculum.

211

212 *Genome-wide Association Scan*

213 We identified genetic variants associated with the onset of autumn torpor by performing
 214 a genome-wide association scan (GWAS) using 46,996 variants with a minor allele frequency
 215 (MAF) ≥ 0.05 and the fit from the linear mixed model. As this was an exploratory analysis using
 216 a relatively small sample set, we set a significance cut-off at $p \leq 5 \times 10^{-4}$. After accounting for
 217 LD, we identified 21 loci that we considered significantly associated with the phenotype (Fig 3A
 218 and Table 3). Although none of the variants met strict genome-wide significance after
 219 *Bonferroni* correction ($p < 1 \times 10^{-6}$), a plot of the observed vs expected quantiles of log-
 220 transformed p-values (Q-Q plot) showed an excess of significant values well above the dashed
 221 line in the tail of the distribution (Fig 3B). Furthermore, while the estimated mean allelic effect
 222 size was -0.04 days (SD=1.84, $n=46,996$), the effect sizes for these 21 significant variants

223 were all within either the top or bottom 1% of the total distribution, being at least ± 4.25 days
 224 for each additional allele (Fig 3C and Table 3).

225

226 **Table 3. Details about the GWAS variants significantly associated with the onset of**
 227 **torpor**

SNP #	Scaffold	Position	Ensembl Scaffold	Ensembl Position	Ref	Alt	MAF	P-value	β	Candidate Gene(s)	Function(s)
1	Scyvm7L_1371	290335	JH393559.1	288921	CA*	C	0.27	2.60E-04	-5.51	RASGEF1 B	GTP signal transduction
2	Scyvm7L_2116	23692482	JH393326.1	1868477	C*	T	0.42	4.73E-05	4.27	MFAP3L; CLCN3	Elastic fiber formation; ion channel transport
3	Scyvm7L_471	7123085	JH393365.1	7103865	GT*	G	0.14	3.71E-04	5.64	NKX2-6	Cardiac embryonic development
4	Scyvm7L_100	29226048	JH393613.1	919871	G*	A	0.31	6.02E-05	-4.71	CDK6; SAMD9	Cell cycle regulation; regulation of cell proliferation and apoptosis
5	Scyvm7L_100	29569341	JH393613.1	1263164	G	T*	0.34	1.54E-04	4.86	FAM133B	Poly(A) RNA-binding
6	Scyvm7L_936	9851454	JH393624.1	94391	G	A* +	0.44	1.33E-04	-5.33	DKK2	Wnt signaling regulation
7	Scyvm7L_146	3229252	JH393286.1	25719306	A	G*	0.16	3.70E-05	-7.45	HLA-DPB1	Peptide antigen binding
8	Scyvm7L_146	3843670	JH393286.1	25104888	G*	A	0.38	7.79E-06	5.37	MLN	Regulation of GI contraction and hunger signaling
9	Scyvm7L_146	5440873	JH393286.1	23507685	G*	A	0.30	3.59E-04	-4.47	CLPS; MAPK14	Fat digestion and satiety; p38 signaling in response to stress
10	Scyvm7L_2912	2711274	JH393389.1	2499372	A	C*	0.46	3.90E-06	5.10	EXOC4; CHCHD3	Insulin response, glucose and lipid uptake; maintenance of mitochondrial cristae
11	Scyvm7L_1866	13078233	JH393463.1	779772	C	A*	0.13	4.91E-04	-6.76	KIAA1324I; GRM3	Unknown; glutamatergic neurotransmission
12	Scyvm7L_1164	849226	JH393548.1	1324176	C*	A	0.10	9.33E-05	-7.95	HPSE; SCD5	Wound healing and coagulation; fatty acid synthesis
13	Scyvm7L_1707	29969722	JH393295.1	2605622	G*	C	0.17	1.80E-04	-5.44	PCSK2	Glucose homeostasis, proinsulin and neuropeptide processing
14	Scyvm7L_607	25116481	JH393369.1	5809915	T	C*	0.22	4.39E-04	-4.75	ZNF462	Transcriptional regulation
15	Scyvm7L_301	9767851	JH393296.1	7909312	C	T*	0.14	3.81E-06	7.32	FAM204A; PRLHR	Unknown; feeding and energy homeostasis
16	Scyvm7L_301	17167980	JH393296.1	15309441	C	T*	0.19	2.77E-05	5.75	FOXI2; PTPRE	Transcriptional regulation; regulation of insulin signaling
17	Scyvm7L_30	2415084	JH393398.1	4077332	C*	A	0.44	4.72E-04	-5.17	Vav1; TRIP10	Immune response; insulin regulated lipid metabolism
18	Scyvm7L_30	2868918	JH393398.1	3623498	C	T* +	0.46	2.14E-04	4.25	ACSBG2	Fatty acyl-CoA biosynthesis
19	Scyvm7L_4270	16068966	JH393402.1	1874622	G	A*	0.48	6.19E-05	5.18	DGKI; PTN	phosphatidic acid production;

20	Scyvm7L_4270	16503923	JH393402.1	1439665	G	T*	0.37	3.20E-05	-5.08	CHRM2	Neurite outgrowth, adipogenesis Regulation of cardiac contractility
21	Scyvm7L_9858	615414	JH393647.1	629692	G*	A	0.37	4.92E-05	5.42	MUC21; DDR1	Cell adhesion; regulation of cell growth

228 Ref is the allele reported in the reference genome assembly

229 * Allele for which effect size is estimated; minor allele unless otherwise specified with +

230 + Major allele

231 MAF is the minor allele frequency estimated from the $n=72$ genotypes used in the association
232 scan

233 β is the effect size estimate in days.

234 Candidate gene(s) are genes nearest to variant; additional genes listed may be functionally
235 related to hibernation.

236

237 We estimated the amount of phenotypic variance explained by the significant loci via
238 linear regression. While the initial model fit with just the fixed effects of sex, year of monitoring
239 and date of hibernaculum placement accounted for 25% of the variance in onset of torpor (Fig
240 4A), these 21 markers explained 54% of the variance (Fig 4B) and when combined with the
241 fixed effects, accounted for 85% of the total variance in the phenotype (Fig 4C). Furthermore,
242 the most significant GWAS variant (SNP 15, Table 3) alone accounted for 21% of phenotypic
243 variance, while the subset of the top five most significant loci (SNPs 15, 10, 8, 16 and 20)
244 explained 47.5% of the variance, excluding fixed effects. Hence, a small subset of markers
245 accounted for most of the genetic component underlying the timing of autumn torpor in this
246 population of 13-lined ground squirrels.

247 When we examined the genes located nearest these significant variants, many were
248 functionally related to themes consistent with physiology underlying the transition to
249 hibernation, such as insulin processing and signaling, feeding and satiety, and control of heart
250 rate (Table 3). Intriguingly, the most significant variant, SNP 15, was located nearest the gene
251 *family with sequence similarity 204 member A (FAM204A)*, whose function is poorly
252 characterized (Fig 5A). However, the *prolactin-releasing hormone receptor (PRLHR)*, involved
253 in stimulating prolactin release and control of feeding [32], and hence more consistent with
254 roles in circannual timing and hibernation, was approximately 270kb from this marker. The
255 second-most significant marker, SNP 10, was located between two genes that are also
256 functionally relevant within the scope of hibernation: *coiled-coil-helix-coiled-coil-helix domain*
257 *containing 3 (CHCHD3)* and *exocyst complex component 4 (EXOC4)*; Fig 5B). While *CHCHD3*
258 maintains the structural integrity of mitochondrial cristae [33], *EXOC4* is a component of the

259 exocyst complex involved in the secretion of insulin [34], as well as lipid and glucose uptake in
260 response to insulin signaling [35,36]. Two weakly-linked variants ($r^2=0.33$) located
261 approximately 500kb from each other, SNP 19 and SNP 20 (Figs 5C & 5D), were near
262 *pleiotrophin (PTN)*, a growth factor involved in neurogenesis and axonal outgrowth,
263 angiogenesis and adipogenesis [37-39], and the *muscarinic acetylcholine receptor M2*
264 (*CHRM2*), which mediates bradycardia in response to parasympathetic-induced acetylcholine
265 release [40], a phenomenon well characterized in hibernation [41,42]. Finally, *motilin (MLN)*, a
266 small peptide hormone that regulates gastrointestinal contractions and stimulates hunger
267 signaling [43] was nearest SNP 8 (Fig 5E), while *prohormone convertase 2 (PCSK2)*, an
268 enzyme that activates hormones and neuropeptides [44-46], including cleavage of proinsulin
269 into its mature form [47], was located in close proximity to SNP 13 (Fig 5F).

270

271 *Identification of eQTLs using transcriptomic datasets*

272 We hypothesized that these significant loci might be linked to gene regulatory variants.
273 We therefore applied an expression quantitative loci (eQTL) analysis using the EDGE-tag
274 transcript datasets from heart, liver, skeletal muscle (SkM) and brown adipose tissue (BAT)
275 [48,49], since a subset of the squirrels genotyped in this study were assayed for transcriptome
276 expression in these prior studies. Under an additive linear model, we identified significant *cis*-
277 eQTL associations ($\pm 500\text{kb}$, $q < 0.1$) for 9/21 variants (Table 4). The most significant GWAS
278 variant, SNP 15, was also the most significant *cis*-eQTL ($q < 4.4 \times 10^{-8}$), where the minor allele,
279 associated with a later onset of torpor (Fig 6A, left plot), was correlated with increased
280 expression of *FAM204A* in BAT (Fig 6A, middle-left and middle-right plots) and SkM. Several
281 variants were associated with expression changes in the previously identified candidate genes
282 (Table 3). SNP 19, associated with a later torpor onset (Fig 6B, left plot), was also correlated
283 with decreased expression of *PTN* in BAT (Fig 6B, middle-left and middle-right plots), while
284 SNP 20, associated with an earlier torpor onset (Fig 6C, left plot), was correlated with
285 increased *CHRM2* expression in heart (Fig 6C, middle-left and middle-right plots). Two
286 variants were correlated with changes in expression of the same transcript in the same
287 direction across tissues: in heart and SkM, SNP 5 correlated with increased expression of
288 *family with sequence similarity 133 member b (FAM133B)*, while SNP 21 correlated with
289 decreased expression of *coiled-coil alpha-helical rod protein 1 (CCHCR1)*; Table 4). In contrast,
290 several variants were associated with expression changes of different transcripts depending on

291 the tissue examined, suggesting their linkage to several regulatory loci within the region or to a
 292 shared regulatory site that exerts its effects on multiple nearby genes [50]. For example, SNP
 293 2 was associated with decreased *chloride voltage-gated channel 3 (CLCN3)* expression in
 294 SkM, yet also associated with increased *microfibril associated protein 3 like (MFAP3L)*
 295 expression in heart (Table 4).

296

297 **Table 4. Details about the significant *cis*-eQTLs**

SNP #	Tissue	Tag ID	Scaffold	Position	Ensembl Scaffold	Ensembl Position	Gene Symbol	Distance (kb)	p-value	q-value	β
2	Heart	Tag_68012	Scyvm7L_2116	23593820	JH393326.1	1967138	MFAP3L	98.7	5.5E-04	0.040	0.76
	SkM	Tag_32453		23802734		1758224	CLCN3	110.3	1.5E-04	0.014	-0.85
5	Heart	Tag_164503	Scyvm7L_100	29572046	JH393613.1	1265869	FAM133B	2.7	1.5E-07	3.1E-05	1.18
	SkM	Tag_78045							1.2E-03	0.071	0.91
8	BAT	Gene_92836	Scyvm7L_146	3382605	JH393286.1	25565906	TAPBP	461.1	2.2E-04	0.011	-0.73
	Heart	Tag_22155		3394532		25554025	ZBTB22	449.1	3.5E-04	0.038	-0.95
13	BAT	Gene_16216	Scyvm7L_1707	30247643	JH393295.1	2327672	LOC106144723	277.9	3.6E-05	3.0E-03	-0.88
15	BAT	Gene_99455	Scyvm7L_301	9806636	JH393296.1	7948097	FAM204A	38.8	1.8E-10	4.4E-08	1.56
	SkM	Tag_16792		9807010		7948471		39.2	1.6E-03	0.071	0.86
17	BAT	Gene_136773	Scyvm7L_30	2440903	JH393398.1	4051486	SH2D3A	25.8	1.4E-05	1.8E-03	-0.69
19	BAT	Gene_137408	Scyvm7L_4270	16236482	JH393402.1	1707078	PTN	167.5	1.1E-04	6.9E-03	-0.67
20	Heart	Tag_114532	Scyvm7L_4270	16416945	JH393402.1	1526642	CHRM2	87.0	1.0E-03	0.056	0.89
	BAT	Gene_79711		299681		299681	MRPS18B	315.7	2.6E-03	0.080	-0.66
21	Heart	Tag_167784	Scyvm7L_9858	810476	JH393647.1	810476	CCHCR1	195.1	1.4E-03	0.059	-0.89
	SkM	Tag_79577							1.1E-04	0.014	-0.97

298 See Table 3 for SNP #

299 Tag ID is from the original Edge-tag datasets in [48,49]

300 β is effect size estimated from quantile-normalized values

301

302 None of the variants met significance thresholds ($q < 0.1$) to be identified as *trans*-eQTLs
 303 (Tables S5-S8); however, this was likely due to the relatively small sample sizes ($n=22-23$ in
 304 heart, SkM and liver; $n=43$ in BAT) and the large number of EDGE-tags tested (25-30K per
 305 tissue) in each dataset. We therefore examined the top *trans*-eGene (>500kb from variant) for
 306 each significant *cis*-eQTL, hypothesizing that we would identify genes within the same pathway
 307 or consistent with the physiology of the *cis*-eGene. Indeed, in heart, the *angiotensin II receptor*
 308 *type 1*, *AGTR1*, involved in regulation of blood pressure [51], was the top *trans*-eGene for SNP
 309 20 ($p=2.97 \times 10^{-5}$, Table S5). In contrast to *CHRM2*, this transcript showed decreased
 310 expression in relation to the minor allele (Fig 6C, right plot), consistent with the physiology of

311 torpor, where reduced heart rate is coupled with decreased blood pressure [52,53]. In BAT, the
312 top *trans*-eGene for SNP 19 was *FER Tyrosine Kinase (FER)*; $p=4.73 \times 10^{-5}$, Table S8), whose
313 expression, like *PTN*, was also decreased in relation to the minor allele of its SNP (Fig 6B,
314 right plot). Both *PTN* and *FER* phosphorylate β -catenin [54,55], suggesting a role for this
315 pathway in the start of torpor. Finally in BAT, the top *trans*-eGene for SNP 15 was *PH domain*
316 *and leucine rich repeat protein phosphatase 1 (PHLPP1)*; $p=2.1 \times 10^{-5}$, Table S8), whose
317 expression, like *FAM204A*, was increased in relation to the variant (Fig 6A, right plot). *PHLPP1*
318 is a protein phosphatase that dephosphorylates and inactivates both *Akt2* and *protein kinase C*
319 [56]. *Akt2* is expressed highly in insulin-responsive tissues, including BAT, where it modulates
320 glucose uptake and homeostasis [57], as well as non-shivering thermogenesis (NST) [58].
321 Moreover, increased *PHLPP1* expression is associated with insulin-resistance and
322 hyperinsulinaemia [59]; hence, this gene may play a role in the switch from glucose to fat-
323 based metabolism that occurs at the onset of seasonal heterothermy, and more specifically in
324 BAT, the regulation of NST.

325

326 Discussion

327 Mammalian hibernation is a highly dynamic and extraordinary phenotype that remains
328 poorly understood. While it has been characterized at behavioral, whole body, cellular, and
329 molecular levels, a genetic basis of the phenotype has yet to be established. Our study is the
330 first, to our knowledge, to characterize genome-wide variation within a hibernator, the 13-lined
331 ground squirrel. This enabled us to estimate the heritability of, and identify genetic variants
332 associated with, the onset of seasonal heterothermy.

333 Our results of heritability are consistent with those from a study that reported significant
334 heritability in spring emersion from hibernation in wild Columbian ground squirrels [60].
335 However, our estimates for immersion into hibernation are much higher. This is likely due to
336 differences between monitoring animals in an animal facility, where environmental conditions
337 and access to food are relatively constant and social cues are minimal, and monitoring animals
338 in the field, where phenotypic plasticity in response to changing environmental conditions also
339 influences phenological timing [61,62]. In the wild, differences in age (adult vs juvenile) and
340 hibernation timing have been observed [61]. While age did not significantly affect hibernation
341 onset in our study, it is worth noting that 74% of the squirrels in this dataset were juveniles,
342 and therefore hibernation-naïve prior to their first torpor bout. Juveniles likely face a far greater

343 challenge in growing and fattening sufficiently to support winter hibernation in the wild; in
344 contrast, in a relatively constant, resource-rich laboratory environment, hibernation onset for
345 these animals may be particularly driven by endogenous mechanisms, thus increasing
346 heritability estimates.

347 In contrast to complex human diseases, where often thousands of variants of relatively
348 small effect influence complex physiological phenotype [63], we find that relatively few loci of
349 large effect account for phenotypic differences in the seasonal onset of hibernation. Our results
350 are comparable to what has been observed for adaptive traits in *A. thaliana* [64], morphological
351 variation in domesticated dogs [65] and plate armor of threespine sticklebacks [66]. This may
352 be simply due to limited sample size, as we were underpowered to detect variants with small
353 effect size and/or at low frequency. However, the results from our ADMIXTURE analysis
354 suggest that wild-trapped founders from two distinct populations were crossed to form the
355 breeding colony. One possible explanation is that torpor onset differs between these two
356 populations, and if so, local genetic adaptation in each could explain the relatively few loci of
357 large effect driving phenotypic variation [67].

358 Although more research is now needed to determine the precise role in torpor
359 immergence for each of these loci, we propose candidate genes, oftentimes the closest to the
360 marker, due to their function being closely related to the physiology of this seasonal transition.
361 In particular, several genes are known to modulate food intake, such as the *prolactin-releasing*
362 *hormone receptor (PRLHR)*, *motilin (MLN)*, and *procolipase (CLPS)* [68]. Researchers have
363 hypothesized that mechanisms governing food intake and metabolic suppression are linked,
364 and that hibernation cannot begin until food intake has ceased [7,69]. Our results support this
365 hypothesis, and present new candidates for study in hibernation.

366 Perhaps the most intriguing candidate gene is *PRLHR*. Sharing a common ancestry
367 with the *NPY* receptors [70], this receptor is expressed primarily in the anterior pituitary, as well
368 as in distinct regions of the brain, including the hypothalamus. Its knockout in mice results in
369 an obese, hyperphagic phenotype, while administration of its agonist, prolactin-releasing
370 hormone (*PRLH*), induces hypophagia and decreases body mass [32]. Both *PRLH* and
371 *PRLHR* appear to mediate the effects of leptin, including activation of NST in BAT [71].
372 Further, *PRLH* belongs to a class of neuropeptides containing a C-terminal RFamide motif
373 [72]; other RFamide-related peptides are involved in circannual regulation of reproduction
374 [73,74]. Binding of *PRLH* to *PRLHR* may induce prolactin release, a hormone that has

375 established roles in the timing of circannual rhythms, such as seasonal molt [75] and
376 reproduction [76]. Moreover, serum prolactin levels coincide with resumption of post-
377 hibernation feeding in marmots [77]. Thus, we hypothesize that *PRLHR* is involved in the
378 regulation of circannual food intake in hibernators; its role in this rhythm warrants further
379 investigation.

380 However, we note that the most significant *cis*-eGene for SNP 15 was not *PRLHR*, but
381 rather its near neighbor, *FAM204A*. This may be due to the marker being linked to several
382 regulatory sites within the region or to a single regulatory site that affects multiple nearby
383 genes. Additionally, *PRLHR*, along with other candidate genes, was not expressed in the
384 tissues for which we had transcriptome data, a limiting factor in our analysis. A role for
385 *FAM204A* in hibernation is unclear, as not much is known about this gene. It appears to be
386 expressed in every tissue and localizes to the nucleus (www.proteinatlas.org [78]), where it
387 interacts with a histone acetyltransferase and a methyltransferase [79]. Therefore, it may play
388 a role in epigenetic regulation of gene expression, possibly in response to the onset of fasting
389 and a switch to fatty acid metabolism [80], as animals prepare for hibernation in the fall.

390 Finally, our results highlight the power of integrating genome data with transcriptome
391 and other high-throughput data to better understand the genetic mechanisms underlying
392 hibernation. Prior “omics” screens (e.g. [10,12,13,22,48,49,81]) have identified hundreds to
393 thousands of genes differentially expressed among the seasonal and physiological states of
394 the hibernator’s year. While leading to insight into the pathways involved, the results of these
395 screens do not distinguish between genes driving vs. those responding to changes in
396 phenotype. They are also limited to the tissue and time-points being examined and may
397 therefore miss important regulators of phenotype. It is worth noting that while several *cis*- and
398 *trans*-eGenes identified here have clear roles in the physiology of torpor, such as *CHRM2* and
399 *AGTR1*, neither of these were identified in their original studies that screened only for
400 differential expression. Thus, by applying complementary genetic mapping approaches,
401 current limitations inherent to gene expression screening strategies will be addressed and
402 enable new insight into the mechanisms driving hibernation. The approaches used here can
403 be extended to a wide variety of hibernators and the quantifiable components that comprise
404 this highly dynamic phenotype.

405

406 **Materials and Methods**

407

408 *Animals*

409 Animals were procured and housed at the University of Colorado, Anschutz Medical Campus,
410 as previously described [15]. All animal use was approved by the University of Colorado,
411 Anschutz Medical Campus, Animal Care and Use Committee.

412 Briefly, 130 colony-bred animals (68 females and 62 males) were obtained from the
413 University of Wisconsin, Oshkosh [82] in the summers of 2007—2010 (Fig 1D, “WI”). These
414 included 73 juveniles naïve to hibernation in the year of study, and 57 adults with at least one
415 year of hibernation. While most from the colony were bred from squirrels originally wild-trapped
416 in northeastern Wisconsin (in and around Oshkosh), several of those obtained from the
417 Oshkosh colony in 2010 were actually bred from either a single or both parents wild-trapped in
418 far western Wisconsin, more than 100 miles away (in and around La Crosse, WI). However,
419 records to identify these specific squirrels were not always maintained. In addition, 17 squirrels
420 (9 females and 8 males; ages unknown), wild-trapped in different locales around central
421 Illinois, were obtained from a commercial supplier (TLS Research, Bloomington, IL) in the
422 summers of 2006 and 2010 (Fig 1D, “IL”). Finally, 6 squirrels (3 females, 3 males; ages
423 unknown) were wild-trapped in the summers of 2006 and 2009 in Elbert County and Larimer
424 County, Colorado (5 and 1, respectively; Fig 1D, “CO”).

425 Upon arrival, animals were housed individually in rodent cages (Fig 1B, bottom) under
426 standard laboratory conditions ($20\pm 2^\circ\text{C}$ and 14:10 light-dark cycle, fed cat chow supplemented
427 with sunflower seeds *ad libitum*). In late August or early September, animals not yet
428 euthanized for tissue collection were surgically implanted with an intraperitoneal datalogger
429 (iButton, Embedded Data Systems) and/or a radiotelemeter (VM-FH disks; Mini Mitter,
430 Sunriver, OR) for remote body temperature (T_b) monitoring until tissue collection. The
431 dataloggers recorded $T_b\pm 0.5^\circ\text{C}$ every 20, 30 or 60 min, while the radiotelemeters transmitted
432 $T_b\pm 0.5^\circ\text{C}$ every 20 sec.

433 In late September or early October, the squirrels were moved to the hibernaculum to
434 facilitate hibernation. The temperature was lowered stepwise over a two-week period to 4°C .
435 Food was removed as animals became torpid.

436

437 *Tissue Collection and Telemeter Retrieval*

438 Liver samples were collected at different points throughout the year for use in other
439 biochemical studies as previously described [19,81,83,84]. All animals were exsanguinated
440 under isoflurane anesthesia, perfused with ice-cold saline, decapitated, and dissected on ice;
441 tissues were immediately snap frozen in liquid nitrogen and stored at -80°C until processed
442 further. Telemeters were retrieved during tissue collection.

443

444 *Body Temperature Telemetry Analysis*

445 To identify the first day of torpor, the telemetry data were analyzed in R [85]. T_b was
446 averaged over 4-hour windows. Homeothermic T_b typically ranged from $34\text{--}39^{\circ}\text{C}$. The first
447 torpor bout was defined as the first point at which T_b fell to or below 25°C (approximately $3\text{--}5^{\circ}\text{C}$
448 above ambient prior to hibernaculum placement, Fig 1C). Most telemetry data continuously
449 logged T_b from the beginning of September of each year. However, in several cases, telemetry
450 recordings did not start until mid-September. Of these, only cases in which first torpor occurred
451 after a minimum of 10 days of continuous monitoring were included for further analysis. In
452 order to merge data across years, date of first torpor was transformed into date from
453 placement into the hibernaculum, which was centered as day 0; hence, all days prior are
454 negative in value, while post-placement dates are positive.

455

456 *HiRise Genome Assembly and Annotation*

457 A Chicago library was prepared as described previously [23] from a single 100mg
458 frozen liver sample. Briefly, $\sim 500\text{ng}$ of high molecular weight gDNA (mean fragment length =
459 $>50\text{kbp}$) was reconstituted into chromatin in vitro and fixed with formaldehyde. Fixed chromatin
460 was digested with *DpnII*, the 5' overhangs filled in with biotinylated nucleotides, and then free
461 blunt ends were ligated. After ligation, crosslinks were reversed and the DNA purified from
462 protein. Purified DNA was treated to remove biotin that was not internal to ligated fragments.
463 The DNA was then sheared to $\sim 350\text{ bp}$ mean fragment size and sequencing libraries were
464 generated using NEBNext Ultra enzymes and Illumina-compatible adapters. Biotin-containing
465 fragments were isolated using streptavidin beads before PCR enrichment of the library. The
466 library was sequenced on an Illumina HiSeq 2500 (rapid run mode) to produce 150 million
467 $2\times 101\text{bp}$ paired end reads, which provided $52.6\times$ physical coverage of the genome ($1\text{--}50\text{kb}$
468 pairs).

469 The 13-lined ground squirrel draft assembly, shotgun reads, and Chicago library reads
470 were used as input data for HiRise, a software pipeline designed specifically for using
471 proximity ligation data to scaffold genome assemblies [23]. Shotgun and Chicago library
472 sequences were aligned to the draft input assembly using a modified SNAP read mapper
473 (<http://snap.cs.berkeley.edu>). The separations of Chicago read pairs mapped within draft
474 scaffolds were analyzed by HiRise to produce a likelihood model for genomic distance
475 between read pairs, and the model was used to identify and break putative misjoins, to score
476 prospective joins, and make joins above a threshold. After scaffolding, shotgun sequences
477 were used to close gaps between contigs. Table S1 describes the input draft assembly
478 scaffold placement within the HiRise scaffolds.

479 Gene annotations from the Ensembl (Release 86) and NCBI (Release 101) datasets
480 were lifted over to the HiRise assembly using a custom Python script and Table S1.

481

482 *Genotype-by-sequencing*

483 We used the modified ddRAD sequencing protocol previously described in [24]. Briefly,
484 high molecular weight DNA was extracted from 8-15 mg of frozen liver with commercially
485 available kits. Digestion and ligation reactions were performed using 200ng of genomic DNA
486 from each sample with *BglII* and *DdeI* and 11-fold excess of sequencing adaptors. Samples
487 were amplified by PCR for 8-12 cycles with a combination of index-containing primers.
488 Between 50-60 samples were pooled in equal amounts according to their concentration of
489 PCR product between 280-480 bp as measured by Tapestation (Agilent Technologies, Santa
490 Clara, CA). Inserts were size-selected on a BluePippin (Sage Science, Beverly, MA) with a
491 target range of 380 ± 100 bp and sequenced on the Illumina NextSeq in single-end 151 bp mode
492 using a high output kit.

493

494 *Variant calling and Filtering*

495 Reads were mapped to the 13-lined ground squirrel HiRise assembly with BWA v.
496 0.7.12. [86]. Tables of predicted *BglII* and *DdeI* restriction digest fragments were generated as
497 described in [24], and sequencing coverage was measured at these sites. We then defined
498 “target regions” for variant calling using the set of fragments between 125-350 bp long that had
499 non-zero coverage in at least one individual. The mapping data are summarized in Table S2.

500 Because publicly available data on 13-lined ground squirrel genetic variation is non-
501 existent, we instead used several variant callers to identify genetic variants and to assess
502 concordance of the genotype calls at each site. Variant calling was performed independently
503 with Sentieon [87], Platypus [88] and Samtools [89,90]. In Sentieon, the pipeline algorithms
504 indel realignment, base quality score recalibration, haplotyper and GVCFTyper were
505 implemented with default settings. In Samtools, variants were called jointly using mpileup to
506 first compute genotype likelihoods and then BCFtools to call genotypes with default
507 parameters. Finally, variants were called jointly in Platypus with the following parameters:
508 minFlank=3, badReadsWindow=5, maxVariants=12, and minReads=6. Only biallelic variants
509 that both passed the filter flags and were identified by all three callers were retained (Fig S3).
510 These variants were next intersected with GATK [91] and compared for genotype call
511 concordance across samples [92]. Those that were $\geq 95\%$ concordant were kept. Basic
512 statistics about the callset, including depth, missingness, heterozygosity, Hardy-Weinberg
513 equilibrium, and TiTv ratio were calculated in VCFtools [93]. Variants with excessive coverage
514 ($\geq 65X$, approx. 4x the mean coverage, Table S2) and heterozygosity (obs./exp. ratio ≥ 1.2)
515 were removed from the callset (Fig S3). Sample libraries with excessive missingness and/or
516 heterozygosity were removed, remade, and resequenced. Variants then were reiteratively
517 called and filtered as described above. Finally, variants present in $\geq 90\%$ of the sample
518 libraries were used for further downstream analyses.

519 *Population Structure and Genetic Relatedness Estimates*

520 We first inferred relatedness from identity-by-state (IBS) estimates among all genotyped
521 squirrels ($n=153$) using KING software [94]. Due to the expectation that the Colorado squirrels
522 are of a separate subspecies [95], relatedness was calculated independently for this subset.
523 We selected an unrelated subset of 54 squirrels that best represented the ancestries of all
524 squirrels within the dataset using the GENESIS package [96] in R [85]. Variants were pruned
525 for LD in PLINK v. 1.9 [97] using the parameters --indep-pairwise 50 10 0.5, which reduced the
526 dataset to 148,870 variants. We then ran unsupervised ADMIXTURE [26] for $K=3$ through
527 $K=10$ with 5-fold cross-validation. To estimate the ancestries of the remaining 99 squirrels, we
528 ran ADMIXTURE's projection analysis using the population structure learned in the initial
529 unsupervised analysis, here with $K=2$ through $K=8$ and 5-fold cross-validation.

530 We performed principal components analyses (PCA) with PLINK using 90,376 LD
531 pruned variants with MAF > 0.01 for the entire dataset and 30,356 LD pruned variants with
532 MAF > 0.01 for the squirrels within the Oshkosh, WI, population ($n=119$), as identified by
533 ADMIXTURE analysis. We extracted the top 20 principal components in each analysis.

534 Finally, we calculated genetic relatedness among the 119 Oshkosh WI squirrels using
535 the GENESIS package, adjusting for both population substructure and inbreeding with the first
536 principal component [29]. We used the resulting kinship coefficients and identity-by-descent
537 (IBD) estimates to reconstruct and visualize pedigrees among the 1st degree relatives with
538 PRIMUS [31]. We also constructed a genetic relatedness matrix from the pairwise kinship
539 coefficients.

540

541 *Genome-Wide Association Scan and Heritability Estimates*

542 All analyses, unless otherwise stated, were performed in R [85]. To identify
543 environmental and biological factors that affected the date of first torpor, we applied a linear
544 regression using variables available from records about the squirrels. In this initial model:
545 Date of first torpor = f(sex + year of monitoring + date of datalogger implantation + age
546 (juvenile vs. adult) + date of placement into hibernaculum + weight (as last recorded before
547 placement into hibernaculum).

548 We then pruned factors using step-wise regression until we identified a minimum set that did
549 not significantly reduce the adjusted R-squared value from the initial model, yet also returned a
550 low AIC value. In this final model:

551 Date of first torpor = f(sex + year of monitoring + date of placement into hibernaculum).

552 These were our fixed effects.

553 We carried out a genome-wide association scan (GWAS) on the date of first torpor
554 using GENESIS [96]. We first fit a linear mixed model using the fixed effects and the genetic
555 relatedness matrix as the random effect. We then performed SNP genotype association tests
556 with 46,996 SNPS (MAF \geq 0.05) and the fit from the linear mixed model. As this was an
557 exploratory analysis, we considered any variant with $p\leq 5\times 10^{-4}$ to be significantly associated
558 with the phenotype. To account for LD, We calculated the r^2 values for significant SNPs within
559 the same scaffold using PLINK [97,98]. We removed those in moderate to high LD ($r^2\geq 0.5$),
560 reporting only the most significant variant.

561 We estimated heritability of the first day of torpor from the variance components of the
562 linear mixed model. In addition, we also estimated heritability of this phenotype using a
563 separate Bayesian mixed model with the MCMCgrm package in R [99]. Here we input the
564 same fixed and random effects (i.e. genetic relatedness matrix) as in the linear mixed model.
565 For the prior, we used an uninformative inverse-gamma distribution (with variance, V , set to 1
566 and belief parameter, ν , set to 0.002) on the variance components. We ran three chains,
567 each with a total of 1,000,000 iterations, a burnin of 100,000 rounds and a thinning interval of
568 200 rounds. Here, all variables had Gelman-Rubin statistics of 1.00 – 1.01, with the absolute
569 value of all autocorrelations < 0.1 and effective sample sizes between 3682.8 and 5294.5. We
570 combined the 3 chains in order to estimate the posterior mode and confidence intervals of the
571 variance components.

572 Finally, we estimated the effects of the significant GWAS variants on the onset of torpor.
573 Specifically, we used linear regression with the phenotype as the dependent variable and a
574 matrix of significant variant genotypes, either with or without the fixed effects, as the
575 explanatory variables. We also performed forward stepwise regression using genotype
576 combinations from the top 10 significant variants.

577

578 *eQTL analysis*

579 We applied an eQTL analysis to identify transcripts whose expression levels were significantly
580 affected by the GWAS variants. Here, we used the EDGE-tag datasets from heart, liver,
581 skeletal muscle (SkM) and brown adipose tissue (BAT) previously described in [48,49], where
582 total RNA was digested with *NlaIII*, resulting in the generation of ≈ 27 -nt “EDGE-tags” [100],
583 which mapped to the 3’UTR’s of transcripts. The squirrels assayed in these prior transcriptome
584 studies were also genotyped in this study: heart ($n=22$), liver ($n=23$), SkM ($n=22$) and BAT
585 ($n=43$). Due to small sample sizes, we limited our eQTL association tests to significant GWAS
586 SNPS with $MAF \geq 0.2$ in heart, liver and SkM and ≥ 0.1 in BAT, which ensured that a minimum
587 of 9 samples contained at least one minor allele.

588 Tests for both *cis*- (± 500 kb) and *trans*-eQTLs were performed with Matrix eQTL [101]
589 under an additive linear model. As the purpose of the original EDGE-tag studies was to identify
590 differentially expressed transcripts among distinct physiological states within the hibernator’s
591 year, we included physiological state as a covariate (5 states in heart, liver and SkM: spring
592 cold, SpC; summer active, SA; interbout-aroused in hibernation, IBA; entering torpor in

593 hibernation, Ent; and late torpor in hibernation, LT; 9 states in BAT, in addition to the those
594 previously mentioned: spring warm, SW; fall transiton, FT; early torpor in hibernation, ET; early
595 in arousal from torpor in hibernation, EAr). In BAT, sequencing platform was also included due
596 to the count bias observed in [49]. Finally, to control for outliers and following
597 recommendations by Matrix eQTL, the counts for each Edge-tag were ranked and quantile-
598 normalized before testing.

599

600 **Acknowledgements**

601 We thank members of the Bustamante Lab for their helpful discussion while this research was
602 being conducted. We also thank R. Russell, A. Hindle and members of the Martin lab who
603 assisted with the 13-lined ground squirrel care, surgical implantation of dataloggers and
604 collection of tissue.

605 C. D. Bustamante is a Chan Zuckerberg Biohub investigator.

606

607 **Funding**

608 This work was supported by the National Science Foundation grant 1642184 to C. D.
609 Bustamante and the National Institutes of Health grant R01HL089049 to S. L. Martin. The
610 funders had no role in study design, data collection and analysis, decision to publish, or
611 preparation of the manuscript.

612

613 **References**

- 614 1. Dark J (2005) Annual lipid cycles in hibernators: integration of physiology and behavior.
615 *Annu Rev Nutr* 25: 469-497.
- 616 2. Pengelley ET (1968) Interrelationships of circannian rhythms in the ground squirrel, *Citellus*
617 *lateralis*. *Comp Biochem Physiol* 24: 915-919.
- 618 3. Pengelley ET, Asmundson SJ, Barnes B, Aloia RC (1976) Relationship of light intensity and
619 photoperiod to circannual rhythmicity in the hibernating ground squirrel, *Citellus*
620 *lateralis*. *Comp Biochem Physiol A Comp Physiol* 53: 273-277.
- 621 4. Ruf T, Geiser F (2015) Daily torpor and hibernation in birds and mammals. *Biol Rev Camb*
622 *Philos Soc* 90: 891-926.
- 623 5. Carey HV, Andrews MT, Martin SL (2003) Mammalian hibernation: cellular and molecular
624 responses to depressed metabolism and low temperature. *Physiol Rev* 83: 1153-1181.
- 625 6. Hampton M, Nelson BT, Andrews MT (2010) Circulation and metabolic rates in a natural
626 hibernator: an integrative physiological model. *Am J Physiol Regul Integr Comp Physiol*
627 299: R1478-1488.
- 628 7. Florant GL, Healy JE (2012) The regulation of food intake in mammalian hibernators: a
629 review. *J Comp Physiol B* 182: 451-467.

- 630 8. Lanaspá MA, Epperson LE, Li N, Cicerchi C, Garcia GE, et al. (2015) Opposing activity
631 changes in AMP deaminase and AMP-activated protein kinase in the hibernating
632 ground squirrel. *PLoS One* 10: e0123509.
- 633 9. Martin SL (2008) Mammalian hibernation: a naturally reversible model for insulin resistance
634 in man? *Diab Vasc Dis Res* 5: 76-81.
- 635 10. Hampton M, Melvin RG, Andrews MT (2013) Transcriptomic analysis of brown adipose
636 tissue across the physiological extremes of natural hibernation. *PLoS One* 8: e85157.
- 637 11. Schwartz C, Hampton M, Andrews MT (2013) Seasonal and regional differences in gene
638 expression in the brain of a hibernating mammal. *PLoS One* 8: e58427.
- 639 12. Hampton M, Melvin RG, Kendall AH, Kirkpatrick BR, Peterson N, et al. (2011) Deep
640 sequencing the transcriptome reveals seasonal adaptive mechanisms in a hibernating
641 mammal. *PLoS One* 6: e27021.
- 642 13. Vermillion KL, Anderson KJ, Hampton M, Andrews MT (2015) Gene expression changes
643 controlling distinct adaptations in the heart and skeletal muscle of a hibernating
644 mammal. *Physiol Genomics* 47: 58-74.
- 645 14. Grabek KR, Martin SL, Hindle AG (2015) Proteomics approaches shed new light on
646 hibernation physiology. *J Comp Physiol B* 185: 607-627.
- 647 15. Russell RL, O'Neill PH, Epperson LE, Martin SL (2010) Extensive use of torpor in 13-lined
648 ground squirrels in the fall prior to cold exposure. *J Comp Physiol B* 180: 1165-1172.
- 649 16. Hindle AG, Martin SL (2014) Intrinsic circannual regulation of brown adipose tissue form
650 and function in tune with hibernation. *Am J Physiol Endocrinol Metab* 306: E284-299.
- 651 17. Hindle AG, Martin SL (2013) Cytoskeletal regulation dominates temperature-sensitive
652 proteomic changes of hibernation in forebrain of 13-lined ground squirrels. *PLoS One* 8:
653 e71627.
- 654 18. Grabek KR, Karimpour-Fard A, Epperson LE, Hindle A, Hunter LE, et al. (2011) Multistate
655 proteomics analysis reveals novel strategies used by a hibernator to precondition the
656 heart and conserve ATP for winter heterothermy. *Physiol Genomics* 43: 1263-1275.
- 657 19. Epperson LE, Rose JC, Carey HV, Martin SL (2010) Seasonal proteomic changes reveal
658 molecular adaptations to preserve and replenish liver proteins during ground squirrel
659 hibernation. *Am J Physiol Regul Integr Comp Physiol* 298: R329-340.
- 660 20. Epperson LE, Rose JC, Russell RL, Nikrad MP, Carey HV, et al. (2010) Seasonal protein
661 changes support rapid energy production in hibernator brainstem. *J Comp Physiol B*
662 180: 599-617.
- 663 21. Epperson LE, Karimpour-Fard A, Hunter LE, Martin SL (2011) Metabolic cycles in a
664 circannual hibernator. *Physiol Genomics* 43: 799-807.
- 665 22. Hindle AG, Grabek KR, Epperson LE, Karimpour-Fard A, Martin SL (2014) Metabolic
666 changes associated with the long winter fast dominate the liver proteome in 13-lined
667 ground squirrels. *Physiol Genomics* 46: 348-361.
- 668 23. Putnam NH, O'Connell BL, Stites JC, Rice BJ, Blanchette M, et al. (2016) Chromosome-
669 scale shotgun assembly using an in vitro method for long-range linkage. *Genome Res*
670 26: 342-350.
- 671 24. Cooke TF, Fischer CR, Wu P, Jiang TX, Xie KT, et al. (2017) Genetic Mapping and
672 Biochemical Basis of Yellow Feather Pigmentation in Budgerigars. *Cell* 171: 427-439
673 e421.
- 674 25. Wang J, Raskin L, Samuels DC, Shyr Y, Guo Y (2015) Genome measures used for quality
675 control are dependent on gene function and ancestry. *Bioinformatics* 31: 318-323.
- 676 26. Alexander DH, Novembre J, Lange K (2009) Fast model-based estimation of ancestry in
677 unrelated individuals. *Genome Res* 19: 1655-1664.

- 678 27. Kurta A, Burt WH (1995) Mammals of the Great Lakes region. Ann Arbor: University of
679 Michigan Press. xii, 376 p. p.
- 680 28. Slatkin M (1993) Isolation by Distance in Equilibrium and Non-Equilibrium Populations.
681 Evolution 47: 264-279.
- 682 29. Conomos MP, Reiner AP, Weir BS, Thornton TA (2016) Model-free Estimation of Recent
683 Genetic Relatedness. Am J Hum Genet 98: 127-148.
- 684 30. Gogarten SM, Bhangale T, Conomos MP, Laurie CA, McHugh CP, et al. (2012)
685 GWASTools: an R/Bioconductor package for quality control and analysis of genome-
686 wide association studies. Bioinformatics 28: 3329-3331.
- 687 31. Staples J, Qiao D, Cho MH, Silverman EK, University of Washington Center for Mendelian
688 G, et al. (2014) PRIMUS: rapid reconstruction of pedigrees from genome-wide
689 estimates of identity by descent. Am J Hum Genet 95: 553-564.
- 690 32. Dodd GT, Luckman SM (2013) Physiological Roles of GPR10 and PrRP Signaling. Front
691 Endocrinol (Lausanne) 4: 20.
- 692 33. Darshi M, Mendiola VL, Mackey MR, Murphy AN, Koller A, et al. (2011) ChChd3, an inner
693 mitochondrial membrane protein, is essential for maintaining crista integrity and
694 mitochondrial function. J Biol Chem 286: 2918-2932.
- 695 34. Tsuboi T, Ravier MA, Xie H, Ewart MA, Gould GW, et al. (2005) Mammalian exocyst
696 complex is required for the docking step of insulin vesicle exocytosis. J Biol Chem 280:
697 25565-25570.
- 698 35. Inoue M, Akama T, Jiang Y, Chun TH (2015) The exocyst complex regulates free fatty acid
699 uptake by adipocytes. PLoS One 10: e0120289.
- 700 36. Inoue M, Chang L, Hwang J, Chiang SH, Saltiel AR (2003) The exocyst complex is
701 required for targeting of Glut4 to the plasma membrane by insulin. Nature 422: 629-633.
- 702 37. Wong JC, Krueger KC, Costa MJ, Aggarwal A, Du H, et al. (2016) A glucocorticoid- and
703 diet-responsive pathway toggles adipocyte precursor cell activity in vivo. Sci Signal 9:
704 ra103.
- 705 38. Perez-Pinera P, Berenson JR, Deuel TF (2008) Pleiotrophin, a multifunctional angiogenic
706 factor: mechanisms and pathways in normal and pathological angiogenesis. Curr Opin
707 Hematol 15: 210-214.
- 708 39. Gonzalez-Castillo C, Ortuno-Sahagun D, Guzman-Brambila C, Pallas M, Rojas-Mayorquin
709 AE (2014) Pleiotrophin as a central nervous system neuromodulator, evidences from
710 the hippocampus. Front Cell Neurosci 8: 443.
- 711 40. Fisher JT, Vincent SG, Gomez J, Yamada M, Wess J (2004) Loss of vagally mediated
712 bradycardia and bronchoconstriction in mice lacking M2 or M3 muscarinic acetylcholine
713 receptors. FASEB J 18: 711-713.
- 714 41. Milsom WK, Zimmer MB, Harris MB (1999) Regulation of cardiac rhythm in hibernating
715 mammals. Comp Biochem Physiol A Mol Integr Physiol 124: 383-391.
- 716 42. Lyman CP (1982) Hibernation and torpor in mammals and birds. New York: Academic
717 Press. x, 317 p. p.
- 718 43. Tack J, Deloof E, Ang D, Scarpellini E, Vanuytsel T, et al. (2016) Motilin-induced gastric
719 contractions signal hunger in man. Gut 65: 214-224.
- 720 44. Toorie AM, Cyr NE, Steger JS, Beckman R, Farah G, et al. (2016) The Nutrient and
721 Energy Sensor Sirt1 Regulates the Hypothalamic-Pituitary-Adrenal (HPA) Axis by
722 Altering the Production of the Prohormone Convertase 2 (PC2) Essential in the
723 Maturation of Corticotropin-releasing Hormone (CRH) from Its Prohormone in Male
724 Rats. J Biol Chem 291: 5844-5859.

- 725 45. Taylor NA, Van De Ven WJ, Creemers JW (2003) Curbing activation: proprotein
726 convertases in homeostasis and pathology. *FASEB J* 17: 1215-1227.
- 727 46. Scriba MF, Ducrest AL, Henry I, Vyssotski AL, Rattenborg NC, et al. (2013) Linking
728 melanism to brain development: expression of a melanism-related gene in barn owl
729 feather follicles covaries with sleep ontogeny. *Front Zool* 10: 42.
- 730 47. Smeekens SP, Montag AG, Thomas G, Albiges-Rizo C, Carroll R, et al. (1992) Proinsulin
731 processing by the subtilisin-related proprotein convertases furin, PC2, and PC3. *Proc*
732 *Natl Acad Sci U S A* 89: 8822-8826.
- 733 48. Bogren LK, Grabek KR, Barsh GS, Martin SL (2017) Comparative tissue transcriptomics
734 highlights dynamic differences among tissues but conserved metabolic transcript
735 prioritization in preparation for arousal from torpor. *J Comp Physiol B* 187: 735-748.
- 736 49. Grabek KR, Diniz Behn C, Barsh GS, Hesselberth JR, Martin SL (2015) Enhanced stability
737 and polyadenylation of select mRNAs support rapid thermogenesis in the brown fat of a
738 hibernator. *Elife* 4.
- 739 50. Tong P, Monahan J, Prendergast JG (2017) Shared regulatory sites are abundant in the
740 human genome and shed light on genome evolution and disease pleiotropy. *PLoS*
741 *Genet* 13: e1006673.
- 742 51. Ito M, Oliverio MI, Mannon PJ, Best CF, Maeda N, et al. (1995) Regulation of blood
743 pressure by the type 1A angiotensin II receptor gene. *Proc Natl Acad Sci U S A* 92:
744 3521-3525.
- 745 52. Horwitz BA, Chau SM, Hamilton JS, Song C, Gorgone J, et al. (2013) Temporal
746 relationships of blood pressure, heart rate, baroreflex function, and body temperature
747 change over a hibernation bout in Syrian hamsters. *Am J Physiol Regul Integr Comp*
748 *Physiol* 305: R759-768.
- 749 53. Lyman CP, O'Brien RC (1963) Autonomic Control of Circulation during the Hibernating
750 Cycle in Ground Squirrels. *J Physiol* 168: 477-499.
- 751 54. Piedra J, Miravet S, Castano J, Palmer HG, Heisterkamp N, et al. (2003) p120 Catenin-
752 associated Fer and Fyn tyrosine kinases regulate beta-catenin Tyr-142 phosphorylation
753 and beta-catenin-alpha-catenin Interaction. *Mol Cell Biol* 23: 2287-2297.
- 754 55. Meng K, Rodriguez-Pena A, Dimitrov T, Chen W, Yamin M, et al. (2000) Pleiotrophin
755 signals increased tyrosine phosphorylation of beta beta-catenin through inactivation of
756 the intrinsic catalytic activity of the receptor-type protein tyrosine phosphatase
757 beta/zeta. *Proc Natl Acad Sci U S A* 97: 2603-2608.
- 758 56. Brognard J, Newton AC (2008) PHLiPPing the switch on Akt and protein kinase C
759 signaling. *Trends Endocrinol Metab* 19: 223-230.
- 760 57. Bouzakri K, Zachrisson A, Al-Khalili L, Zhang BB, Koistinen HA, et al. (2006) siRNA-based
761 gene silencing reveals specialized roles of IRS-1/Akt2 and IRS-2/Akt1 in glucose and
762 lipid metabolism in human skeletal muscle. *Cell Metab* 4: 89-96.
- 763 58. Albert V, Svensson K, Shimobayashi M, Colombi M, Munoz S, et al. (2016) mTORC2
764 sustains thermogenesis via Akt-induced glucose uptake and glycolysis in brown adipose
765 tissue. *EMBO Mol Med* 8: 232-246.
- 766 59. Andreozzi F, Procopio C, Greco A, Mannino GC, Miele C, et al. (2011) Increased levels of
767 the Akt-specific phosphatase PH domain leucine-rich repeat protein phosphatase
768 (PHLPP)-1 in obese participants are associated with insulin resistance. *Diabetologia* 54:
769 1879-1887.
- 770 60. Lane JE, Kruuk LE, Charmantier A, Murie JO, Coltman DW, et al. (2011) A quantitative
771 genetic analysis of hibernation emergence date in a wild population of Columbian
772 ground squirrels. *J Evol Biol* 24: 1949-1959.

- 773 61. Sheriff MJ, Kenagy GJ, Richter M, Lee T, Toien O, et al. (2011) Phenological variation in
774 annual timing of hibernation and breeding in nearby populations of Arctic ground
775 squirrels. *Proc Biol Sci* 278: 2369-2375.
- 776 62. Sheriff MJ, Richter MM, Buck CL, Barnes BM (2013) Changing seasonality and
777 phenological responses of free-living male arctic ground squirrels: the importance of
778 sex. *Philos Trans R Soc Lond B Biol Sci* 368: 20120480.
- 779 63. Manolio TA, Collins FS, Cox NJ, Goldstein DB, Hindorff LA, et al. (2009) Finding the
780 missing heritability of complex diseases. *Nature* 461: 747-753.
- 781 64. Atwell S, Huang YS, Vilhjalmsdottir BJ, Willems G, Horton M, et al. (2010) Genome-wide
782 association study of 107 phenotypes in *Arabidopsis thaliana* inbred lines. *Nature* 465:
783 627-631.
- 784 65. Boyko AR, Quignon P, Li L, Schoenebeck JJ, Degenhardt JD, et al. (2010) A simple
785 genetic architecture underlies morphological variation in dogs. *PLoS Biol* 8: e1000451.
- 786 66. Colosimo PF, Peichel CL, Nereng K, Blackman BK, Shapiro MD, et al. (2004) The genetic
787 architecture of parallel armor plate reduction in threespine sticklebacks. *PLoS Biol* 2:
788 E109.
- 789 67. Savolainen O, Lascoux M, Merila J (2013) Ecological genomics of local adaptation. *Nat*
790 *Rev Genet* 14: 807-820.
- 791 68. Erlanson-Albertsson C, York D (1997) Enterostatin--a peptide regulating fat intake. *Obes*
792 *Res* 5: 360-372.
- 793 69. Davis DE (1976) Hibernation and circannual rhythms of food consumption in marmots and
794 ground squirrels. *Q Rev Biol* 51: 477-514.
- 795 70. Lagerstrom MC, Fredriksson R, Bjarnadottir TK, Fridmanis D, Holmquist T, et al. (2005)
796 Origin of the prolactin-releasing hormone (PRLH) receptors: evidence of coevolution
797 between PRLH and a redundant neuropeptide Y receptor during vertebrate evolution.
798 *Genomics* 85: 688-703.
- 799 71. Dodd GT, Worth AA, Nunn N, Korpak AK, Bechtold DA, et al. (2014) The thermogenic
800 effect of leptin is dependent on a distinct population of prolactin-releasing peptide
801 neurons in the dorsomedial hypothalamus. *Cell Metab* 20: 639-649.
- 802 72. Elphick MR, Mirabeau O (2014) The Evolution and Variety of RFamide-Type
803 Neuropeptides: Insights from Deuterostomian Invertebrates. *Front Endocrinol*
804 (Lausanne) 5: 93.
- 805 73. Kriegsfeld LJ (2006) Driving reproduction: RFamide peptides behind the wheel. *Horm*
806 *Behav* 50: 655-666.
- 807 74. Wood S, Loudon A (2017) The pars tuberalis: The site of the circannual clock in
808 mammals? *Gen Comp Endocrinol*.
- 809 75. Lincoln GA, Clarke IJ, Hut RA, Hazlerigg DG (2006) Characterizing a mammalian
810 circannual pacemaker. *Science* 314: 1941-1944.
- 811 76. Tortorella DJ (2016) Intrapituitary mechanisms underlying the control of fertility: key
812 players in seasonal breeding. *Domest Anim Endocrinol* 56 Suppl: S191-203.
- 813 77. Concannon PW, Castracane VD, Rawson RE, Tennant BC (1999) Circannual changes in
814 free thyroxine, prolactin, testes, and relative food intake in woodchucks, *Marmota*
815 *monax*. *Am J Physiol* 277: R1401-1409.
- 816 78. Uhlen M, Fagerberg L, Hallstrom BM, Lindskog C, Oksvold P, et al. (2015) Proteomics.
817 Tissue-based map of the human proteome. *Science* 347: 1260419.
- 818 79. Chatr-Aryamontri A, Oughtred R, Boucher L, Rust J, Chang C, et al. (2017) The BioGRID
819 interaction database: 2017 update. *Nucleic Acids Res* 45: D369-D379.

- 820 80. McDonnell E, Crown SB, Fox DB, Kitir B, Ilkayeva OR, et al. (2016) Lipids Reprogram
821 Metabolism to Become a Major Carbon Source for Histone Acetylation. *Cell Rep* 17:
822 1463-1472.
- 823 81. Hindle AG, Grabek KR, Epperson LE, Karimpour-Fard A, Martin SL (2014) The liver
824 proteome in hibernating ground squirrels is dominated by metabolic changes associated
825 with the long winter fast. *Physiol Genomics*.
- 826 82. Merriman DK, Lahvis G, Jooss M, Gesicki JA, Schill K (2012) Current practices in a captive
827 breeding colony of 13-lined ground squirrels (*Ictidomys tridecemlineatus*). *Lab Anim*
828 (NY) 41: 315-325.
- 829 83. Nelson CJ, Otis JP, Martin SL, Carey HV (2009) Analysis of the hibernation cycle using
830 LC-MS-based metabolomics in ground squirrel liver. *Physiol Genomics* 37: 43-51.
- 831 84. Rose JC, Epperson LE, Carey HV, Martin SL (2011) Seasonal liver protein differences in a
832 hibernator revealed by quantitative proteomics using whole animal isotopic labeling.
833 *Comp Biochem Physiol Part D Genomics Proteomics* 6: 163-170.
- 834 85. R Core Team (2016) R: A Language and Environment for Statistical Computing. Vienna,
835 Austria: R Foundation for Statistical Computing.
- 836 86. Li H, Durbin R (2009) Fast and accurate short read alignment with Burrows-Wheeler
837 transform. *Bioinformatics* 25: 1754-1760.
- 838 87. Freed D, Aldana R, Weber J, Edwards J (2017) The Sentieon Genomics Tools - A fast and
839 accurate solution to variant calling from next-generation sequence data. *bioRxiv*.
- 840 88. Rimmer A, Phan H, Mathieson I, Iqbal Z, Twigg SRF, et al. (2014) Integrating mapping-,
841 assembly- and haplotype-based approaches for calling variants in clinical sequencing
842 applications. *Nat Genet* 46: 912-918.
- 843 89. Li H (2011) A statistical framework for SNP calling, mutation discovery, association
844 mapping and population genetical parameter estimation from sequencing data.
845 *Bioinformatics* 27: 2987-2993.
- 846 90. Li H, Handsaker B, Wysoker A, Fennell T, Ruan J, et al. (2009) The Sequence
847 Alignment/Map format and SAMtools. *Bioinformatics* 25: 2078-2079.
- 848 91. McKenna A, Hanna M, Banks E, Sivachenko A, Cibulskis K, et al. (2010) The Genome
849 Analysis Toolkit: a MapReduce framework for analyzing next-generation DNA
850 sequencing data. *Genome Res* 20: 1297-1303.
- 851 92. Cingolani P, Patel VM, Coon M, Nguyen T, Land SJ, et al. (2012) Using *Drosophila*
852 *melanogaster* as a Model for Genotoxic Chemical Mutational Studies with a New
853 Program, SnpSift. *Front Genet* 3: 35.
- 854 93. Danecek P, Auton A, Abecasis G, Albers CA, Banks E, et al. (2011) The variant call format
855 and VCFtools. *Bioinformatics* 27: 2156-2158.
- 856 94. Manichaikul A, Mychaleckyj JC, Rich SS, Daly K, Sale M, et al. (2010) Robust relationship
857 inference in genome-wide association studies. *Bioinformatics* 26: 2867-2873.
- 858 95. Armstrong DM (1971) Notes on Variation in *Spermophilus tridecemlineatus* (Rodentia,
859 Sciuridae) in Colorado and Adjacent States, and Description of a New Subspecies.
860 *Journal of Mammalogy*, 52: 528-536.
- 861 96. Matthew P. Conomos, Timothy Thornton, Gogarten SM (2017) GENESIS: GENetic
862 ESTimation and Inference in Structured samples.
- 863 97. Chang CC, Chow CC, Tellier LC, Vattikuti S, Purcell SM, et al. (2015) Second-generation
864 PLINK: rising to the challenge of larger and richer datasets. *Gigascience* 4: 7.
- 865 98. Shaun Purcell, Chang C PLINK 1.9.
- 866 99. Hadfield J (2010) MCMC Methods for multi-response generalized linear mixed models: The
867 MCMCglmm R Package. *Journal of Statistical Software* 33: 1-22.

- 868 100. Hong LZ, Li J, Schmidt-Kuntzel A, Warren WC, Barsh GS (2011) Digital gene expression
869 for non-model organisms. *Genome Res* 21: 1905-1915.
870 101. Shabalin AA (2012) Matrix eQTL: ultra fast eQTL analysis via large matrix operations.
871 *Bioinformatics* 28: 1353-1358.
872 102. IUCN (International Union for Conservation of Nature) 2016. *Ictidomys tridecemlineatus*.
873 The IUCN Red List of Threatened Species. 2017-2 <http://www.iucnredlist.org>.
874 Downloaded on 12 June 2017
875

876 **Supporting Information Captions**

877 **Fig S1. Comparison of the contiguity of the input assembly and the final HiRise**
878 **scaffolds.** Each curve shows the fraction of the total length of the assembly in scaffolds of a
879 given length or smaller. The fraction of the assembly is indicated on the Y-axis and the scaffold
880 length in basepairs is given on the X-axis. The two dashed lines mark the N50 and N90
881 lengths of each assembly. This plot excludes scaffolds less than 1 kb.
882

883 **Table S1. Details of the draft assembly input and orientation into the final HiRise**
884 **assembly**
885

886 **Fig S2. HiRise assembly improves the scaffold N50: 539 draft assembly scaffolds are**
887 **reduced to 33.** Each bar represents a HiRise scaffold. Each color within the bar represents a
888 draft assembly scaffold. Note: colors are used to show placement of input scaffolds but are not
889 specific to any one scaffold. Number of draft input scaffolds are listed on right.
890

891 **Table S2. Summary mapping results for each ddRADseq library**
892

893 **Fig S3. Variant calling pipeline and results.** (A) The Venn diagram (top) shows the number
894 of unique and shared variants detected by Platypus, Sentieon and SamTools variant callers.
895 The flow chart beneath outlines the filtering strategy and the number of retained variants after
896 each filtering step. (B) For the 884,092 variants detected by and passing filter flags in each
897 variant caller, plot shows the mean proportion of variant calls that were concordant (Concord),
898 discordant (Discord) or Missing between Sentieon and Platypus (Plat) and Sentieon and
899 SamTools (SamT) among all samples as a function of coverage. Blue box highlights criterion
900 range of $\leq 65x$ coverage. (C) The observed versus expected heterozygosity ratio of each
901 variant, represented as an open circle and plotted by minor allele frequency (MAF). Those with

902 a ratio >1.2 , above the black horizontal line, were filtered from the dataset. Each variant is
903 colored according to its Hardy-Weinberg equilibrium test statistic p-value bin listed in the
904 legend (top left of plot). (D) For the 575,178 variants passing all filtering steps, the plot shows
905 the mean proportion of variant calls that were concordant (Concord), discordant (Discord) or
906 Missing between duplicate libraries of 4 samples (two samples from UW OshKosh, WI,
907 “OK.TR1” and “OK.TR2”; and two samples from IL, “IL.TR1” and “IL.TR2”) as a function of
908 coverage.

909

910 **Fig S4. ADMIXTURE 5-fold cross-validation (CV) error for each value of K .** Shown are the
911 CV error values for $K=2$ through $K=8$.

912

913 **Table S3. Pairwise F_{ST} estimates for the $K=6$ ADMIXTURE populations.**

914 See text for labeling.

915

916 **Fig S5. Principal components PC17 and PC19 of all 153 genotyped squirrels reveal**
917 **population structure within the OshKosh subset of squirrels.** Coloring is the same as in
918 Fig 2A and 2C.

919

920 **Table S4: Biological and environmental data for each Oshkosh squirrel in which torpor**
921 **onset was recorded**

922

923 **Table S5. Heart *trans*-eQTL results**

924 Table lists results for all *trans*-eqtl associations with $p \leq 1 \times 10^{-5}$

925 See Table 3 for SNP #

926 Tag ID is from the original Edge-tag datasets in [48,49]

927 β is effect size estimated from quantile-normalized values

928

929 **Table S6. SkM *trans*-eQTL results**

930 Labeling is the same as in Table S5

931

932 **Table S7. Liver *trans*-eQTL results**

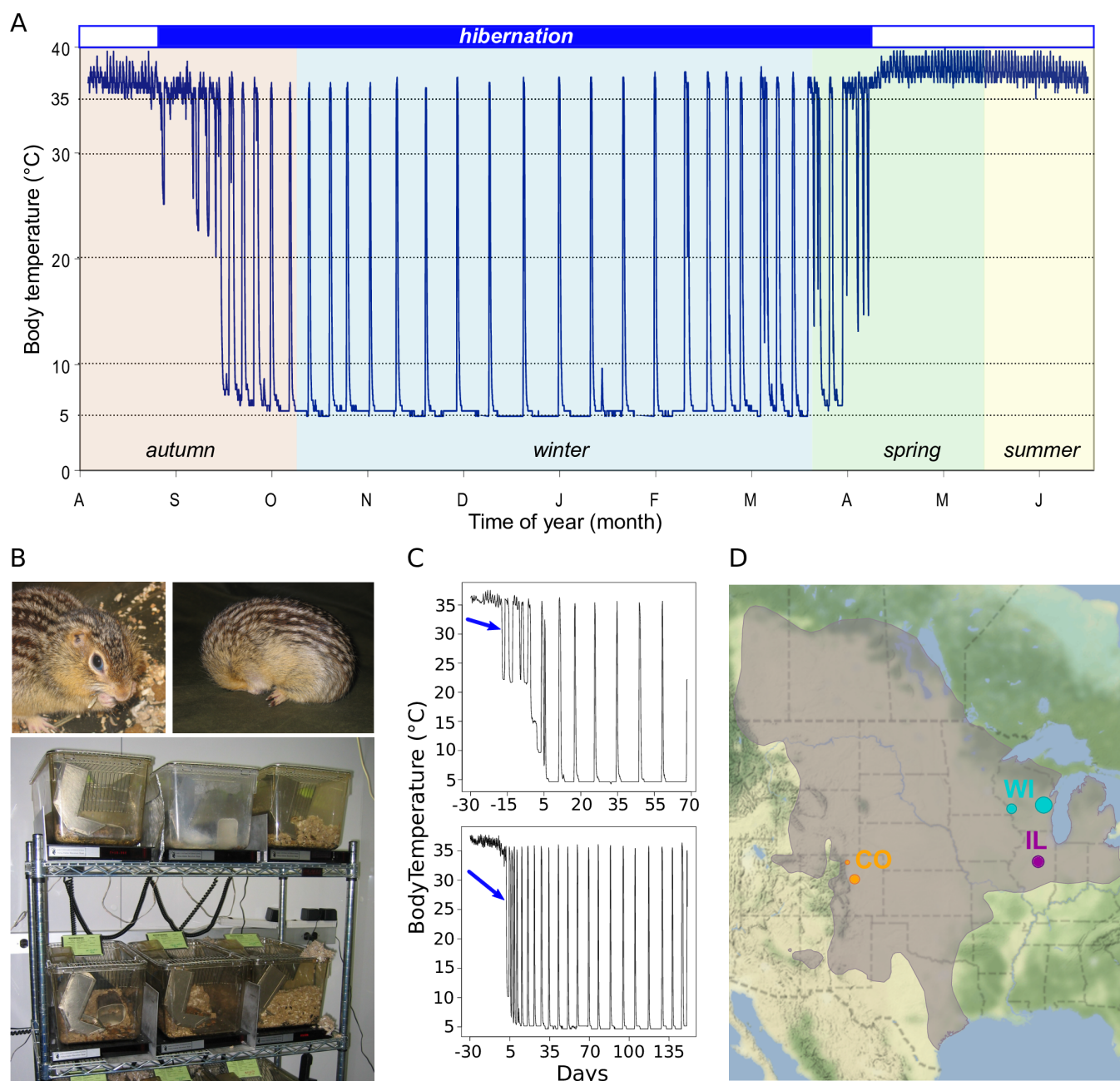
933 Labeling is the same as in Table S5

934

935 **Table S8. BAT *trans*-eQTL results**

936 Labeling is the same as in Table S5

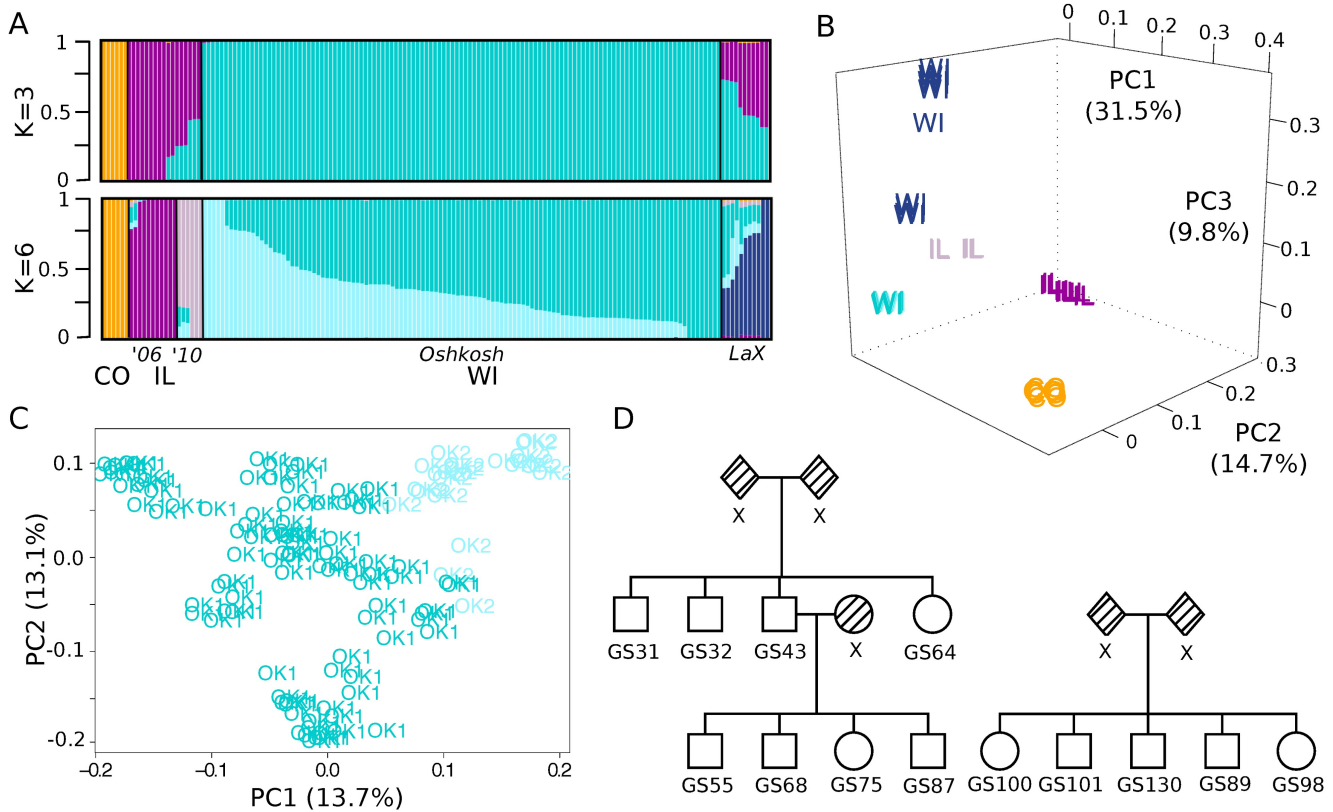
937



938

939 **Fig 1. The 13-lined ground squirrel as a model for studying the genetics of hibernation.**

940 (A) Body temperature trace showing a 13-lined ground squirrel's year. Hibernating portion is
941 demarcated by blue shaded box above. (B) A non-hibernating (top left) and hibernating (top
942 right) 13-lined ground squirrel, individually housed in standard lab rodent cages in an animal
943 facility (bottom). (C) Representative plots of body temperature telemetry analyses. Arrows
944 point to the first day of torpor, the phenotype measured in this study. Days are \pm from
945 hibernaculum placement. (D) Approximate locales of squirrels genotyped in this study. Shaded
946 area indicates the 13-lined ground squirrel's geographic range [102].



947

948

949

950

951

952

953

954

955

956

957

958

959

960

Fig 2. Genotype-by-sequencing reveals population structure and relatedness among sampled squirrels. (A) ADMIXTURE analysis results showing $K=3$ or $K=6$ genome-wide specific ancestry estimates. Squirrels are shown as vertical bars with proportion of specific ancestry colored within each bar. Populations are clustered and labeled by geographic sampling locales (U.S. state, and for WI, city) and for those from IL, sampling years. (B) Principal components analysis of all 153 genotyped squirrels. The first 3 PCs are plotted, with individuals labeled by state and colored by the population for which they have the greatest proportion of ancestry as determined by $K=6$ ADMIXTURE analysis shown in (A). (C) Principal components analysis of 119 squirrels from the Oshkosh WI population. The first 2 PCs are plotted with individuals labeled and colored by Oshkosh sub-population (OK1 or OK2) as determined by $K=6$ ADMIXTURE analysis shown in (A). (D) Representative pedigrees reconstructed from identity by descent (IBD) and kinship coefficient estimates of the Oshkosh squirrels. Shaded shapes labeled "x" indicate relatives not genotyped in this study.

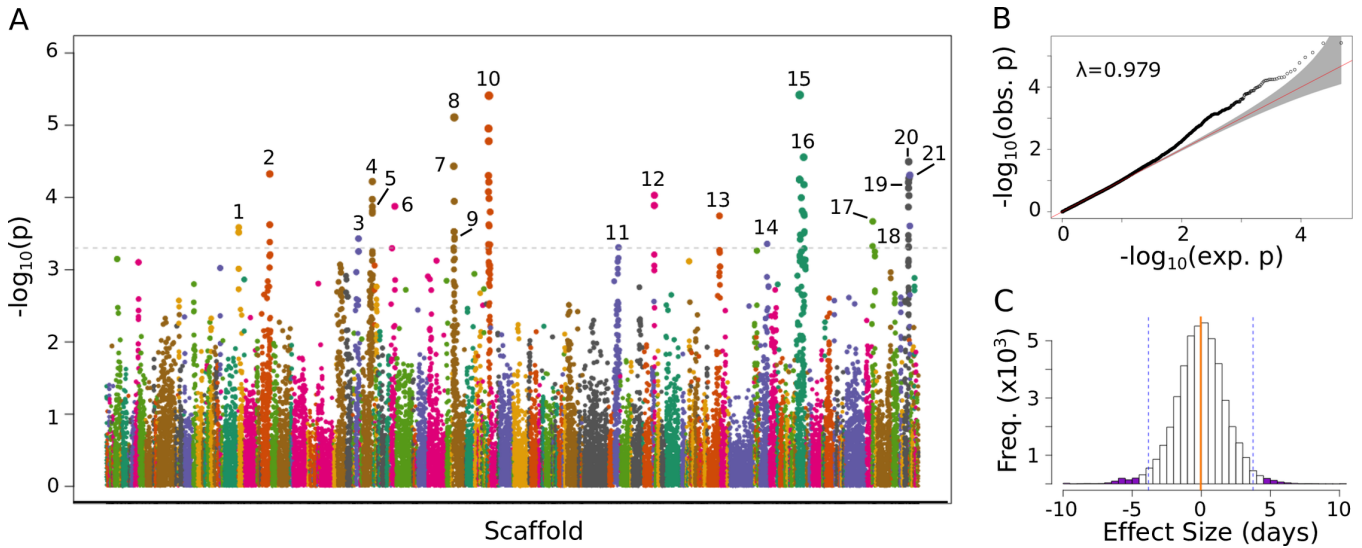
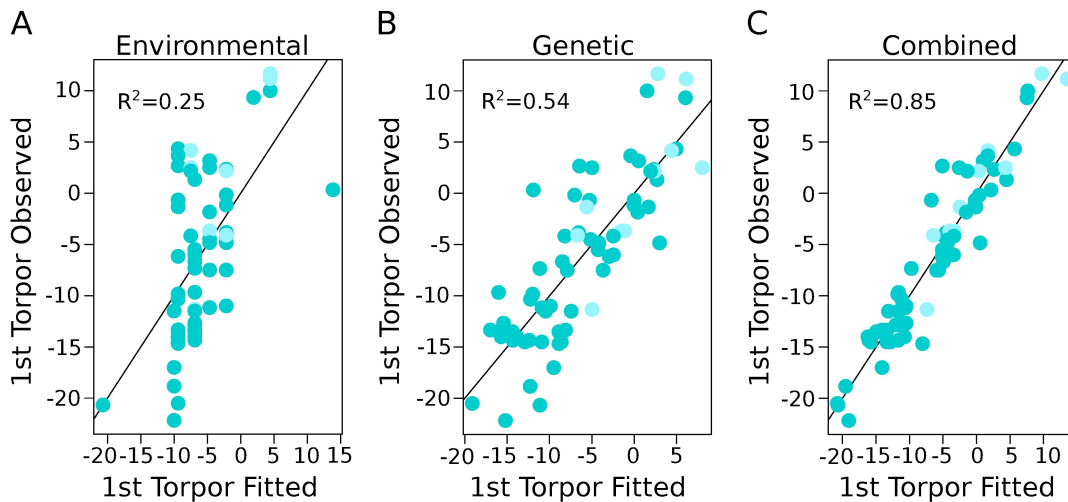


Fig 3. GWAS identifies genetic variants significantly associated with date of first torpor in 13-lined ground squirrels. (A) Manhattan plot shows the negative log-transformed p-values of 46,996 variants (MAF>0.05) tested for association with date of first torpor in 72 squirrels. Variants are ordered by position on scaffold, which are colored along x-axis. Dashed line indicates cutoff for significance ($p < 5 \times 10^{-4}$). Significantly associated variants, pruned for LD, are numbered and correspond to those detailed in Table 3 and in Figs 5 and 6. (B) Q-Q plot of the GWAS log-transformed p-values. (C) Histogram of effect sizes of the 46,996 variants on date of first torpor. Orange vertical line marks the mean, dashed vertical lines mark upper and lower bounds of 98th percentile and purple shading indicates effect sizes of the 21 significantly associated variants.



972

973

974

975

976

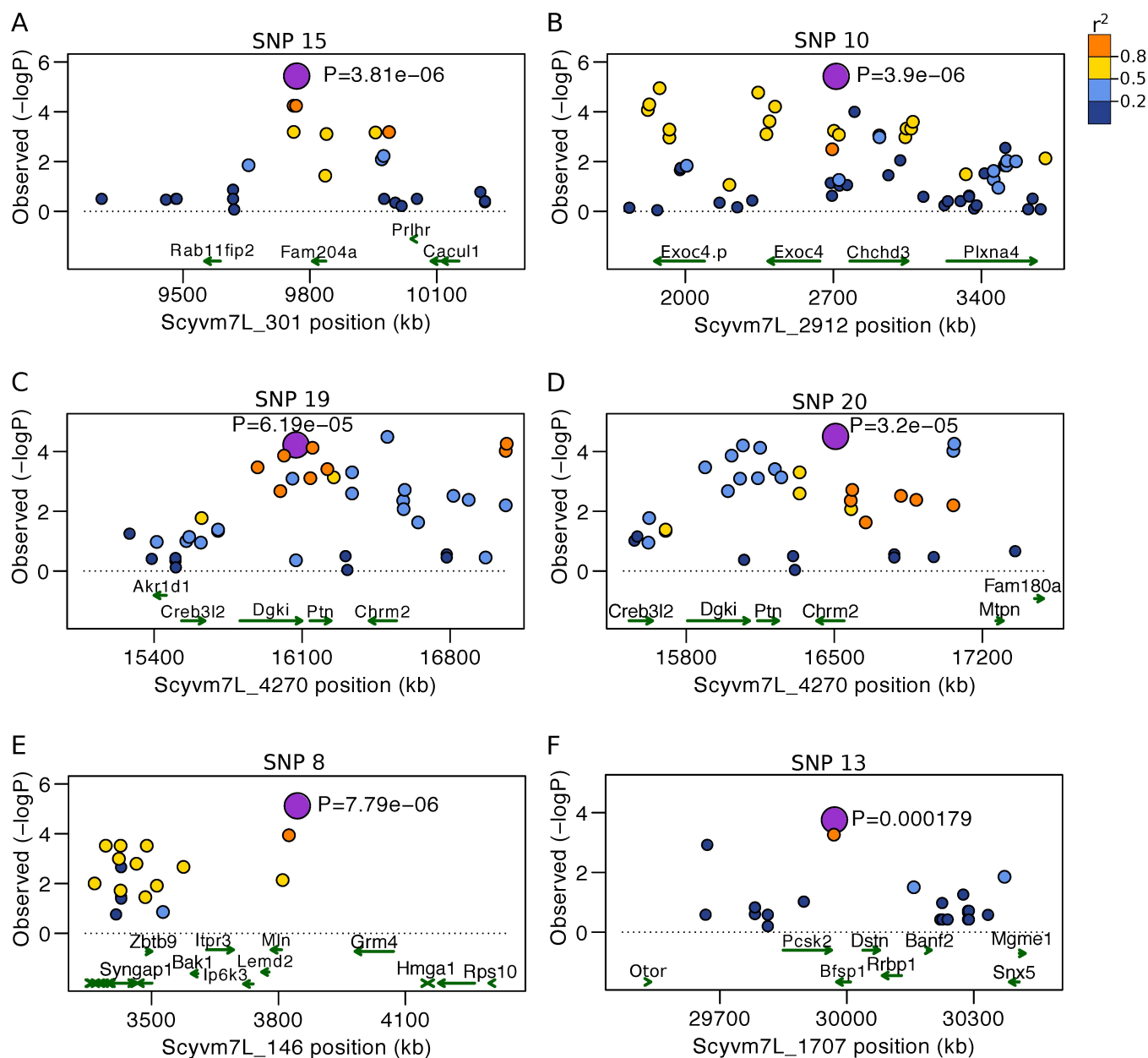
977

978

979

980

Fig 4. Combined environmental and genetic effects account for variation in the start of torpor. Plots show correlation between fitted and observed values for the start of torpor (in days from hibernaculum placement) using a linear regression model. Adjusted R^2 -value is labeled in each. Shading matches Figs 2A and 2C. (A) Linear model fit with the environmental variables of year of monitoring and date of hibernaculum placement, and the biological variable of sex (i.e. the “fixed effects”, see methods). (B) Linear model fit with the 21 significant SNP genotype combinations for each squirrel. (C) Linear model fit with the variables from both (A) and (B).



981

982 **Fig 5. Regional Manhattan plots show locations of selected significant SNPs in**

983 **proximity to nearest genes.** Each plot is centered on one of the significant SNPs, which are

984 labeled on top by number (see Fig 3A and Table 3) and shaded purple. Other variants within

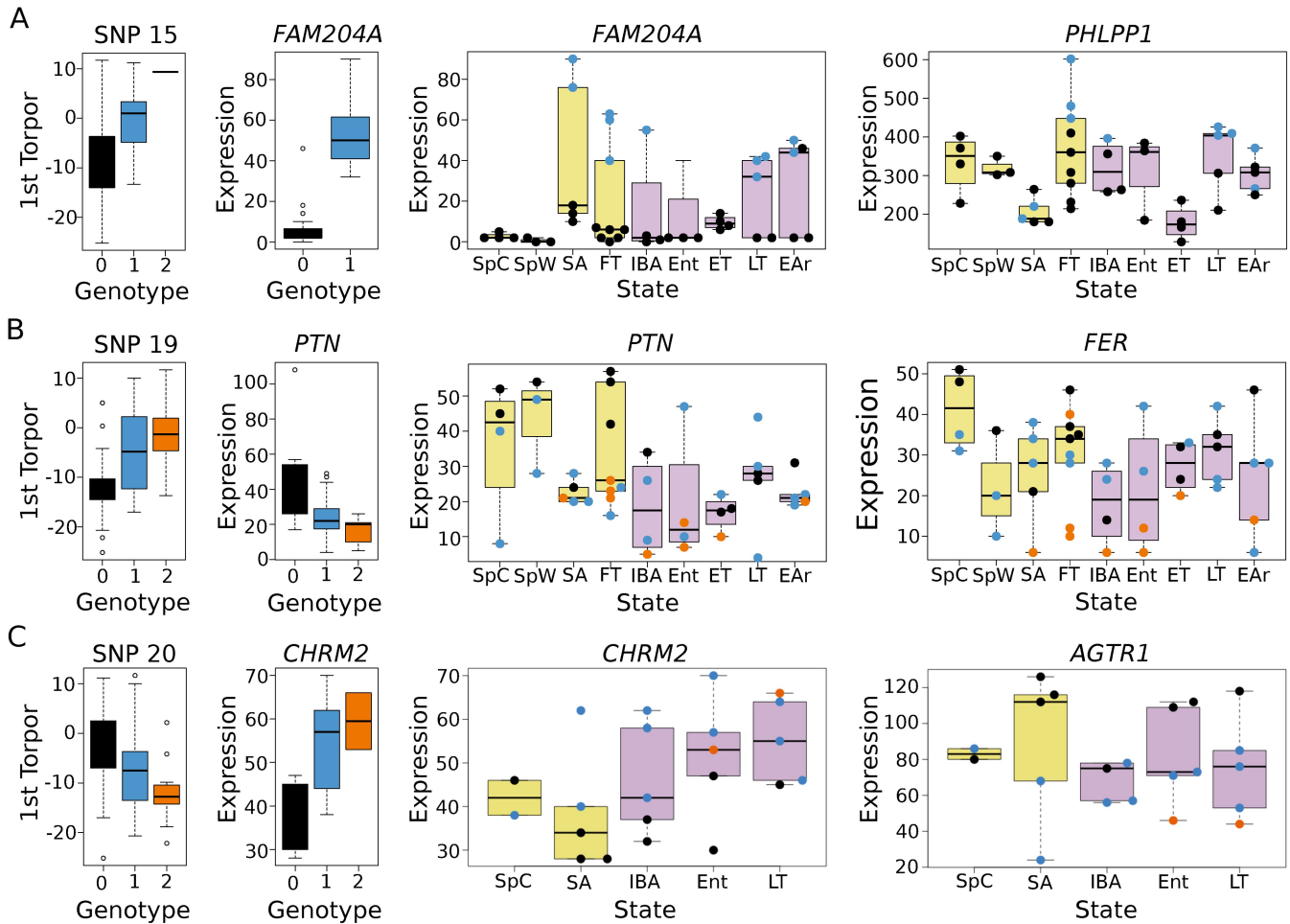
985 region are colored by LD value (r^2) in relation to the significant SNP. Genes are shown below

986 as green arrows and labeled by gene symbol. (A) SNP 15, the most significant SNP in the

987 GWAS, is nearest *FAM204A*. (B) SNP 10, the second most significant SNP, is between

988 *CHCHD3* and *EXOC4*. (C) SNP 19 is located nearest *DGKI* and *PTN*. (D) SNP 20 is located

989 nearest *CHRM2*. (E) SNP 9 is nearest *MLN*. (F) SNP 13 is between *PCSK2* and *BFSP1*.



990

991 **Fig 6. Significant GWAS SNPs are also *cis*- and *trans*-eQTLs that explain variation in**

992 **mRNA expression. (A) Effect of SNP 15 genotype on date of first torpor (far left) and**

993 **expression of its *cis*-eGene, *FAM204A*, in BAT (middle left). Middle right plot shows effect of**

994 **genotype on transcript expression within each of the nine distinct physiological and seasonal**

995 **states interrogated in the original transcriptome study (labeled below, see methods for**

996 **explanation of sampling abbreviations). Shaded yellow boxes indicate physiological states**

997 **from homeothermic and transitional portions of hibernator's year (spring-autumn), while purple**

998 **shaded boxes are those from within deep hibernation. Far right plot shows effect of genotype**

999 **on expression of the most significant *trans*-eGene, *PHLPP1*. (B-C) Labeling is as in panel (A).**

1000 **(B) Effect of SNP 19 on *cis*-eGene *PTN* and *trans*-eGene *FER* in BAT. (C) Effect of SNP 20 on**

1001 ***cis*-eGene *CHRM2* and *trans*-eGene *AGTR1* in heart.**

1002